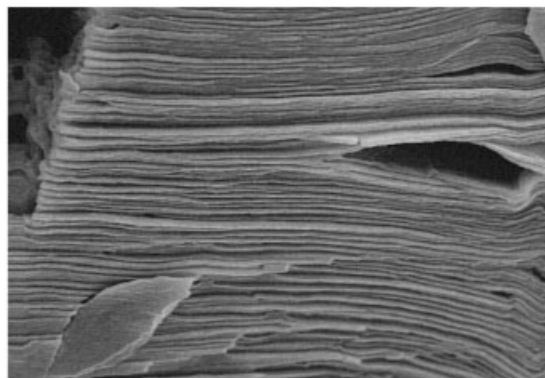


Summary: The unusual structure of poly(ethylene oxide) (PEO) and Laponite clay in transparent nanocomposite films was investigated using scanning electron, atomic force, and optical microscopy, and X-ray scattering. Each method is sensitive to different aspects of structural features and together they measure the resulting morphology and shear-induced orientation. On nanometer length scales, clay platelets were found to orient in bundles while polymer crystallinity was suppressed. Microscopy led to the observation of unexpected and highly oriented multilayers on the micron length scale.

Scanning electron microscopy image of the freeze-fractured surface of a poly(ethylene oxide)–Laponite film: the view on top of the x – y plane.



Unusual Multilayered Structures in Poly(ethylene oxide)/Laponite Nanocomposite Films

Avinash Dundigalla,¹ Sheng Lin-Gibson,² Vincent Ferreiro,³ Matthew M. Malwitz,¹ Gudrun Schmidt*¹

¹Department of Chemistry, Louisiana State University, Baton Rouge, LA 70803, USA

Fax: (+1) 225 578 3458; E-mail: gudrun@lsu.edu

²Polymers Division, National Institute of Standards and Technology, Gaithersburg, MD 20899-8543, USA

³Laboratoire de Structure et Propriétés de l'Etat Solide, UMR CNRS 8008, Université des Science et Technologie de Lille, Villeneuve d'Ascq, France

Received: October 18, 2004; Revised: November 18, 2004; Accepted: November 19, 2004; DOI: 10.1002/marc.200400489

Keywords: Laponite; microscopy; nanocomposites; poly(ethylene oxide) (PEO); X-ray

Introduction

Highly ordered polymer nanocomposites are complex materials that display a rich morphological behavior because of variations in composition, structure, and properties on a nanometer length scale.^[1,2] When combining materials over length scales ranging from 1–10 nm, the interface of the components becomes substantially important to the materials' performance.^[3] Organizing clay platelets of high-aspect ratios at the nanometer length scale is, thus, a challenging and rewarding research area in materials science.^[4]

Several solution and melt fabrication techniques leading to materials with intercalated to exfoliated structures have been used for the preparation of poly(ethylene oxide) (PEO)–clay nanocomposites. Since both the untreated clay and PEO are hydrophilic, no clay surface modification is necessary for complete exfoliation in aqueous solution. Moreover, PEO has been found to penetrate into both Laponite and montmorillonite clay and promote the exfoliation process in aqueous solutions. However the strong interac-

tions between the two components often lead to aggregation that is difficult to avoid.^[5] It has been observed that after air drying of solutions, the clay particles remain trapped in a gel-like polymer film reminiscent of the exfoliated polymer clay gel in the “wet state”.^[2] The film quality can be improved by slow solvent evaporation where the clay platelets have sufficient time to assemble under gravitational and osmotic forces before the viscosity of the system influences particle realignment.^[6] An industrially promising method is the melt intercalation of polymer into clay where the polymer chains have been shown to be more effectively intercalated than in solution.^[7] New methods are being developed for the fabrication of molecularly ordered composite films by self-assembly that may replace the Langmuir–Blodgett techniques.^[8,9] Multilayered films have been prepared by sequential adsorption of polymer and clay.^[10] Atomic force microscopy (AFM) on some of these multilayered films revealed that polymer–Laponite clay films exhibit significantly higher surface coverage than montmorillonite clays.^[8]

We are interested in the fabrication of highly oriented PEO-Laponite nanocomposite films from the corresponding aqueous gels. Previous work relevant to this contribution described rheological^[11] and small-angle neutron scattering (SANS)^[12] studies on PEO-clay network-like solutions and gels. In solution, the polymer and clay interact in a dynamic adsorption/desorption equilibrium to form a three-dimensional network.^[13] The network mesh size and the orientation of the clay platelets in solution are important to the structures of the dried films. We also examined the orientation of platelets in multilayered polymer-Laponite and polymer-montmorillonite films^[14] by small- and wide-angle scattering.^[15]

The objectives of the present contribution are to prepare nanocomposite films with a defined orientation of the Laponite clay platelets from network-like polymer-clay gels. We will examine the film structural features on multiple length scales using various scattering and microscopy techniques. Only completely dried films were investigated. On a nanometer length scale, small-angle (SAXS) and wide-angle X-ray scattering (WAXS), and AFM was used to study the structure and shear-induced orientation of polymer and platelets in a complementary fashion. Scanning electron microscopy (SEM) and optical microscopy investigate the morphology of the films on a micron length scale. We also compare our results to previously reported PEO/montmorillonite multilayered films.^[14]

Experimental Part

Laponite (LRD) is a synthetic Hectorite-type clay consisting of relatively monodisperse and well-defined platelets with a diameter of 25–30 nm and a thickness of approximately 1 nm (Southern Clay Products). Poly(ethylene oxide) (PEO) with an $\bar{M}_w = 10^6$ g·mol⁻¹ and a molecular mass distribution of approximately 1.5 was purchased from Polysciences Inc. Multilayered films were prepared by gel/solution exfoliation, while optimal solutions were obtained for a particular polymer clay ratio. pH and ionic strength are as previously described by Schmidt et al.^[11–13] and Malwitz et al.^[14] Here, multilayered films will be discussed that have been prepared from an aqueous gel containing mass fractions of 3% LRD clay and 2% PEO at ambient temperature. The solution pH and ionic strength were controlled by the addition of NaOH (pH = 10) and NaCl (1×10^{-3} M), respectively. Gels were spread onto glass slides layer-by-layer and dried at 25 °C in desiccators and under vacuum. Multilayered films containing approximately 60% of Laponite clay and 40% of PEO polymer (by mass fraction) were obtained. A more detailed film preparation is described elsewhere.^[15] Time-resolved small-angle X-ray scattering (SAXS) and wide-angle X-ray scattering or diffraction (WAXS) measurements were performed at the Advanced Polymers Beamline at the National Synchrotron Light Source (NSLS), Brookhaven National Laboratory. Optical microscopy was performed using an Olympus BX51TF microscope with crossed polarizers. SEM experiments were performed using a Cambridge 260 Stereoscan Electron Microscope. Frac-

tures in all three planes were investigated and only representative images are presented. Sample preparation for the AFM measurements included cryo-ultramicrotome slicing (Leica ultracut with FC4 from Reichert–Jung). Samples were cut at –120 °C, below the PEO glass transition temperature ($T_g = -55$ °C). The images were recorded with a Nanoscope IIIa (Veeco Instruments).^[16] Duplicate measurements on all instruments show excellent reproducibility with a relative uncertainty of less than 5%.

Results and Discussion

The structure and properties of the PEO-Laponite nanocomposite films strongly depend on their morphology, polymer-clay interactions, and shear orientation. Our previous work on PEO-Laponite solutions and gels demonstrated that in the wet state, the polymer chains are entangled with the clay particles forming a transient network.^[11–13] Similar results were observed for PEO-montmorillonite gels.^[17] The solution structure and processing conditions strongly influence the morphology of the dried film. Rheological experiments on PEO-Laponite gels for those used in the films' preparation have shown that the Laponite clay platelets align at low shear rates, and after cessation of shear, rapidly relax from alignment.^[17] The collapse of network structure as the solution dries likely leads to highly oriented layers in the dried film.

X-ray Scattering and AFM

The physical picture of the clay platelet orientation as concluded by the WAXS is illustrated in Figure 1a. The isotropic patterns in the x - z plane and the anisotropy observed in the x - y plane suggest that the predominant orientation of platelets is with the surface normal perpendicular to the film plane (x - z plane) (Figure 1). From the two-dimensional (2D) SAXS and WAXS patterns, the intensity as a function of q can be calculated in x , y , and z directions. The SAXS intensity in the x and y direction of the 2D SAXS pattern (Figure 1) is shown in Figure 2a. A maximum at $q_{\max} \approx 0.01$ Å⁻¹ corresponds to a d spacing, $d_{\text{SAXS}} = 2\pi/q_{\max}$, in the order of approximately 63 nm. This value is approximately two times the clay diameter (30 nm) and may be related to a distance between polymer-covered clay-rich domains containing several platelets. Comparable SANS experiments on these films also show $d_{\text{SANS}} \approx 63$ nm but with less resolution, because of smearing from the form factor.^[15] It is interesting to note that a PEO-montmorillonite film containing 40% of clay (different clay type and clay size) will show a very similar d spacing and layer size, but the layer nanostructure is very different when observed with AFM.^[14]

Figure 2b displays the relative intensity versus 2θ , as obtained from WAXS shown in Figure 1. Intensities were calculated in the x , y , and z directions. The scattering profile

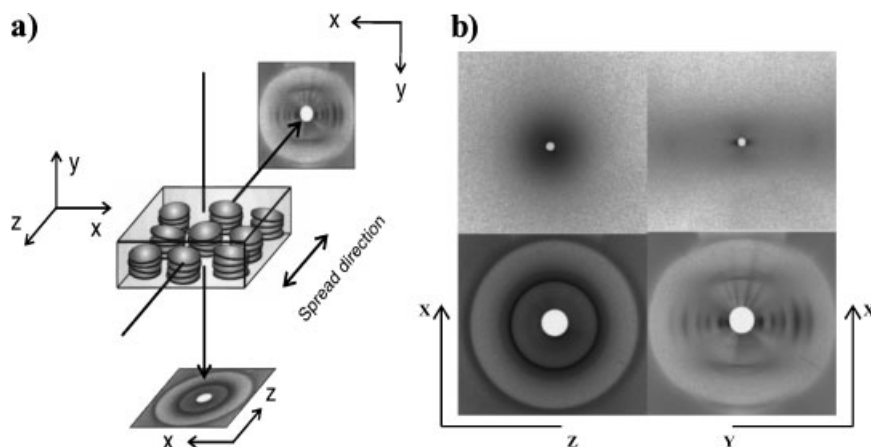


Figure 1. a) With the clay platelets aligned in the spread direction of the film (x - z plane) we observe an anisotropic WAXS pattern with the X-ray beam oriented in a z configuration, and an isotropic WAXS pattern with the beam oriented in a y configuration; b) SAXS and WAXS measured parallel and perpendicular to the spread direction of the films. Top row: SAXS in the x - z plane (left) and x - y plane (right). Bottom row: WAXS in the x - z plane (left) and x - y plane (right).

obtained in the y direction is significantly different from those obtained in the x and z directions, indicating that this sample is highly oriented. The typical crystalline structure of pure PEO is a well-known monoclinic lattice, with the WAXS normally showing several orders of diffraction. However, here we do not observe any peaks originating from PEO crystals. The peaks observed in the WAXS y direction mainly correspond to distances between the clay platelets within the clay-rich domains or clay stacks. The PEO adsorbed to the clay is thus mostly amorphous.

The d spacing obtained from present SAXS and previous SANS^[15] ($d \approx 63$ nm) experiments can be correlated with the spacing of the striped texture as measured from AFM $d_{\text{AFM}} \approx 66$ nm (average over many measured spacings, Figure 3). The domain distance is marked by arrows on the micrograph (Figure 3). These domains consist of intercalated stacks of platelets; however, it is not possible to determine from AFM alone how many clay platelets are inside one domain. Planned transmission electron microscopy may visualize the content of one single domain. The anisotropic SAXS pattern (Figure 1) can be correlated with the fast Fourier-transform AFM data, which shows a broad anisotropic streak perpendicular to the striped texture (Figure 3, top right). AFM data show two kinds of layers: nanometer size layers and micron thick layers. Micron thick layers may be compared with SEM data shown in Figure 4a.

On similar length scales, AFM and SAXS are complementary methods. SAXS yields reciprocal space information and an average degree of orientation, while AFM visualizes real space structures within discrete sections of the sample. This explains the slight differences in d_{AFM} and d_{SAXS} spacings. However, the existence of the ordered and layered structure observed with AFM is unusual. The orientation of clay platelets with a diameter of approximately 30 nm and a thickness of 1 nm does not explain the

presence of ordered layers with an average thickness of 63 nm (Figure 3). We presume that the 63 nm layers correspond to clay domains or the clay stack layers mentioned above. The x direction correlation length observed in the AFM image (Figure 3) is approximately 25–30 nm and corresponds to the clay diameter. The clay particles can only adsorb a maximum amount of polymer until all the clay surfaces are covered. Any excess polymer in solution as well as in the bulk leads to formation of network-like polymer-clay phases and polymer-rich phases.^[7,18] During the drying and spreading process, these two phases lead to the layered structure observed with AFM and SAXS. This interpretation is consistent with similar behavior of bulk nanocomposites observed in the literature.^[7,13,18] It should be noted that the films need to be kept in a desiccator, since both the clay and polymer are hygroscopic and reversible absorption/desorption of water may lead to swelling or shrinking of the polymer, thereby increasing or decreasing the layer spacing. This is a property that makes the material applicable as a potential humidity sensor.^[19]

Crystallinity, as determined by differential scanning calorimetry (DSC), changed from near 0 to 3% within one year. The WAXS data shown in Figure 2b and described earlier confirm that the adsorbed PEO is mostly amorphous. From our preliminary microscopy and scattering results, and from the literature^[20] on polymer clay solutions, we know that the PEO polymer chains strongly adsorb to the clay particles. The adsorbed polymer layer was calculated to be approximately 1.5 nm on each side, increasing the average thickness of a wrapped clay platelet from a total of 1 nm (thickness of the clay platelet) to approximately 4 nm (polymer wrapped clay platelet). If the domains visualized by AFM contain only stacked and wrapped platelets, one approximately 63 nm thick domain would contain a maximum of approximately 15 platelets ($4 \text{ nm} \times 15 = 60 \text{ nm}$).

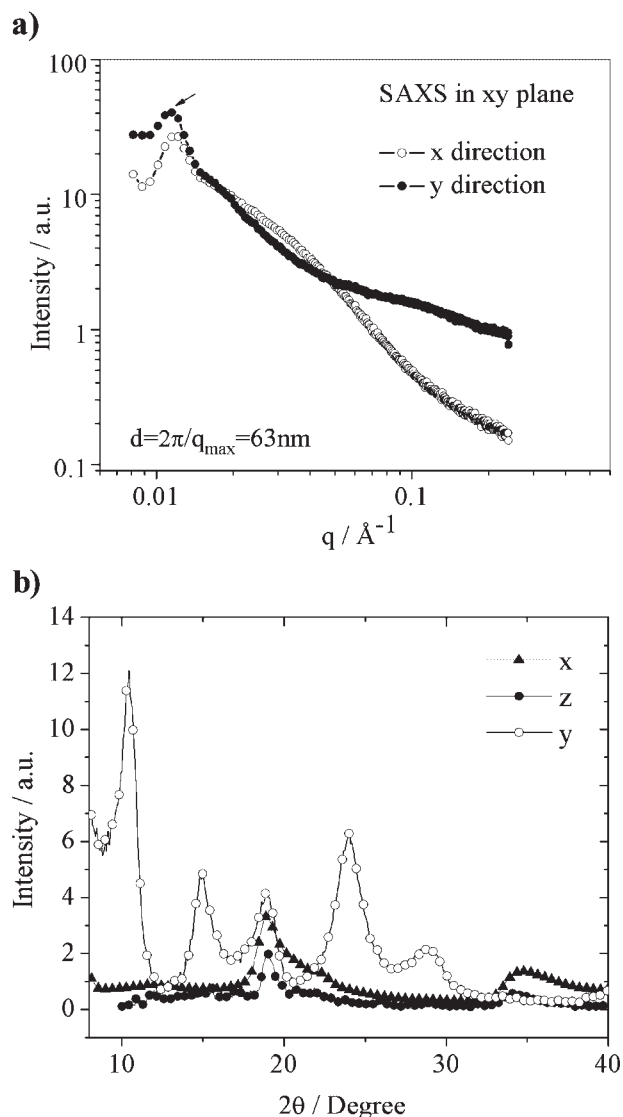


Figure 2. a) SAXS intensity in the x and y directions. A maximum in SAXS gives a characteristic dimension of $d_{\text{SAXS}} = 2\pi/q_{\text{max}} = 63$ nm; b) WAXD pattern measured in the x , y , and z directions.

The minimum distance between these wrapped platelets would be approximately 3 nm (adsorbed polymer layer on each side = $1.5 \text{ nm} \times 2$). However, defects and excess polymer that is not absorbed to the clay particles may reduce the number of platelets inside one domain. WAXS data in the y direction do not show a “perfect” lamellar order of 1:2:3:4 in q (momentum transfer), thus complicating the structural information. Further experiments and data evaluation is necessary to quantify these results.

Scanning Electron Microscopy

SEM was used to determine the film morphology on the micron length scale (Figure 4a,b). As mentioned previously, the aqueous PEO–Laponite gels can be described as inter-

connected networks. When the solvent was evaporated, the network collapsed and films were obtained with layered structures that can be observed on several length scales. In the x – y plane of the films (Figure 4a), SEM was used to examine whether an interface exists between spread layers. Similar to PEO–montmorillonite films that we have studied previously,^[14] no boundaries between spreading layers (each 5–7 μm) could be detected, indicating substantial intermixing of spread layers. Nevertheless a highly ordered and layered structure of the films was observed in the x – y plane, while smooth and flat surfaces were observed in the x – z plane (Figure 4b). The few broad layers visible come from an imperfect fracture along the x – z plane. The layered texture of the x – y SEM image is not uniform and was calculated to have an average dimension of $d_{\text{SEM}} \approx 0.3 \pm 0.17 \mu\text{m}$ per layer. Even though the exact shear rate during the spreading process cannot be controlled, SEM shows high reproducibility in data. According to AFM and SAXS measurements, each of the approximately 0.3 μm thick layers consists of smaller layers that are on average 60 nm thick (Figure 3 and 4). As a result of processing conditions, that is, drying and layer-by-layer spreading, we also observe clusters of smaller domains and some larger aggregates. Several AFM images in the horizontal and vertical distances must be probed to observe these structures. The layer structures observed by SEM are considerably smaller than the calculated width of a single layer spread to form the nanocomposite film. Defects and fracture of the film (Figure 4) show smooth surfaces between layers as well as some folding of layers. This suggests that strong interconnectivity between the polymer and clay produces large flat surfaces. Although we observe structures on the micron length scales, all these films were completely transparent in the dry state. Optical transparency of samples with micron size texture is usually possible when refractive index matching of the large scale structures is present.

From the smooth fracture visible in Figure 4 (and from other SEM images not shown here), we conclude that the polymer–clay interactions parallel to the micron size layers are not as strong as those perpendicular to the layers. Inspection of several SEM images also suggests that a fractured sample preferentially breaks parallel to the layered structure. This is influenced by the formation of two-phase nanocomposites and suggests that there may be excess polymer between layers. The network-like polymer–clay intercalates and the polymer-rich phases in between layers may not need to have strong interconnections since the clay can adsorb only a maximum amount of polymer until all the clay surfaces are covered. Any excess polymer in solution and in the bulk is not directly cross-linked to the clay particles but covers the polymer–clay aggregates.

We conclude that the strength of the polymer–clay network in solution strongly influences the alignment of polymer and clay during the spreading process. The

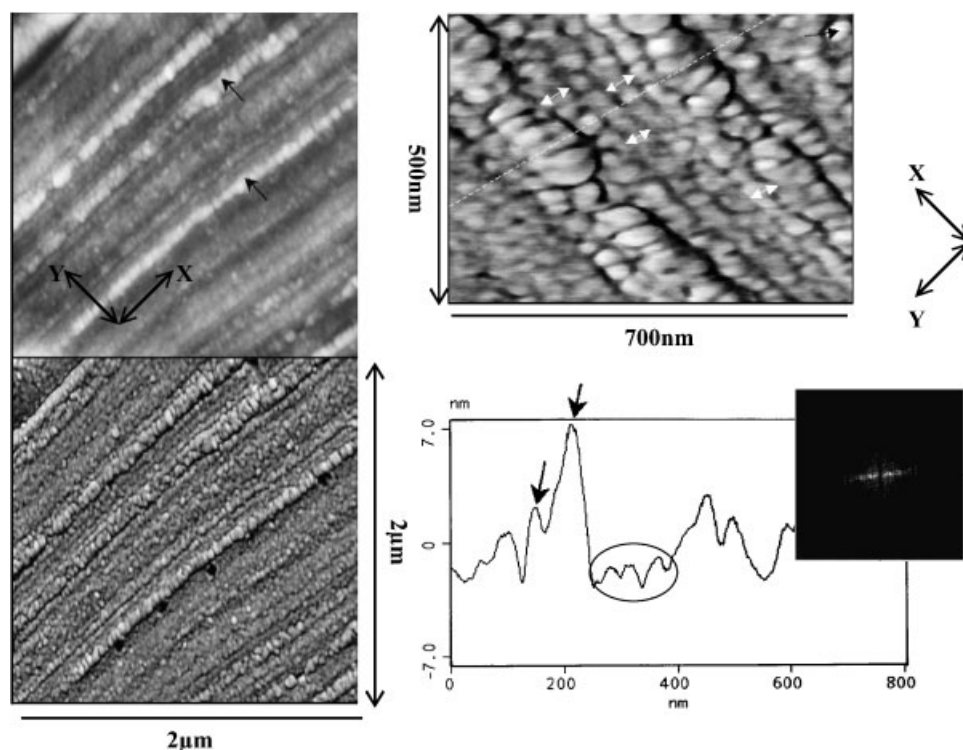


Figure 3. Left: AFM images from the x - y plane sections of multilayered film. Top) ($2\ \mu\text{m} \times 2\ \mu\text{m}$) AFM “height” image. Bottom) ($2\ \mu\text{m} \times 2\ \mu\text{m}$) AFM “Phase” image. The vertical grey scale is 50° . Right: Top) ($700\ \text{nm} \times 500\ \text{nm}$) AFM “Phase” image of the details of multilayered structure. The vertical grey scale is 25° . Arrows indicate the width of the individual layers. Bottom) Cross section of the corresponding “height” image of the above AFM image. The direction of the cross section is indicated in the above AFM image by the dotted white line. The two arrows show thick layers. The dotted black circle shows three individual layers lying perpendicular to the film surface. FFT shows the regularity of the multilayer structure that can be compared with the SAXS data shown in Figure 2 top right.

collapse of the network during the spreading and drying process of the films reduces the pore sizes and the shear leads to orientation and anisotropy as well as structural changes. While in solution, the clay is completely exfoliated; the dried film shows significant change in structure. One example is the presence of domains containing several clay platelets in a stacked order (Figure 3). Although the relaxation in solution is very fast, we assume that it is the shear combined with the slow drying of thin layers within a concentration gradient that leads to the orientation. An ongoing study will try to determine the rate of drying for locking in the orientation versus the relaxation. Preliminary results show that a thick polymer clay film that has not been sheared but only dried is brittle, porous, and cloudy. The spreading and drying procedure influences both the micro- and macrostructure and transparency. Evaporation of the solvent at ambient temperature combined with shear orientation strongly improved the film quality and the mechanical properties (as compared with a non-sheared and non-layered thick film) and increased the orientation of clay platelets that are layered between the polymer.

Optical Microscopy

The macrostructure of the transparent films was also characterized by polarized microscopy, which showed differences in birefringence in each plane (Figure 4c,d). A small section of a one-layer film was removed (by scratching or cutting) to expose the x - y plane. The x - z plane did not show birefringence, which indicates there is little polymer crystallinity in the x - z plane. Any existing PEO crystallites that are not detectable by WAXS and DSC are also not large enough to be detected by optical microscopy. With increasing temperatures ranging from 25 to 200°C , the birefringence of the x - y plane gradually fades because of melting of oriented polymer chains. Observation of the exposed edge of the film, the x - y plane, shows some birefringent pattern even after annealing for one hour at 200°C . The total birefringence of the film is dominated by the orientation of the clay platelets and possibly stretched polymer chains within the sample. Stretched polymer chains in confinement do not necessarily need to be crystalline. Since the polymer is almost amorphous (according

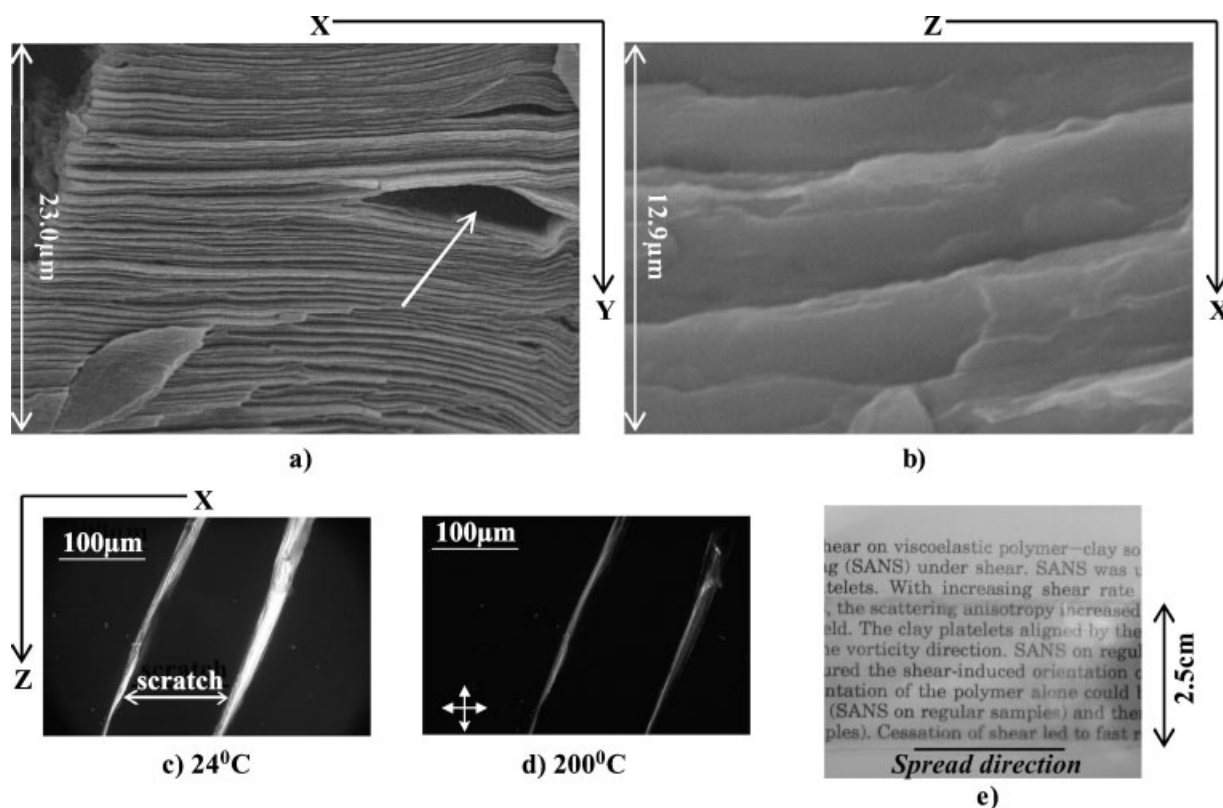


Figure 4. SEM images of freeze-fractured surfaces: a) SEM view on top of the x - y plane, b) SEM view on top of the x - z plane. Planes are described in Figure 1. c,d) Optical micrograph of a transparent nanocomposite film with a scratched surface. A small section of a one-layer film was removed to expose the x - y plane. Crossed polarizers and a magnification of 20 were used. e) Transparent nanocomposite film of 1 mm thickness.

to WAXS and DSC), birefringence may be somewhat influenced by shear effects during the scratching or cutting of the film. We believe that at high temperatures birefringence comes from the clay alone, while at low temperatures both polymer and clay contribute to total birefringence in the x - y plane.

Conclusion

Previous work on bulk PEO-nanocomposites has shown that it is difficult to increase the clay intergallery spacing beyond a certain distance by adding more polymer to the system, and that excess polymer will phase separate upon the removal of water.^[6,14] Our recent work on PEO-montmorillonite multilayered films (clay content: 40%) has shown excess polymer to phase separate within highly ordered nanometer-sized layers.^[14] The present study on PEO-Laponite films (clay content: 60%) shows additional periodicity within nanometer-sized layers (Figure 3). As the water evaporates during the film preparation, the electrolyte concentration increases, causing phase separation of PEO at higher concentrations. The presence of salt is in part responsible for the development of the unusual layered

structures. Differential scanning calorimetry suggests that the high concentration of Laponite clay (60%) is sufficient to suppress the PEO crystallization. Films with high clay contents may be used as precursors for ceramic materials or microelectronics. The crystallinity of various bulk PEO nanocomposites at much lower clay concentrations has been extensively studied in the past.^[6,21] The suppression or induction of crystallinity in confinement is very important in controlling the structure in our multilayered films, issues that the authors will address in future research.

Disclaimer

Certain commercial materials and equipment are identified in this paper in order to adequately specify the experimental procedure. In no case does such identification imply recommendation by the National Institute of Standards and Technology nor does it imply that the material or equipment identified is necessarily the best available for this purpose.

According to ISO 31-8, the term molecular mass has been replaced by relative molecular mass (\bar{M}_r). Hence, if this nomenclature and notation were to be followed, one would write \bar{M}_{rw} , instead of the historically conventional \bar{M}_w , for

the mass-average average relative molecular mass. The conventional notation rather than the ISO notation has been employed for this publication.

Acknowledgements: We acknowledge financial support in part from an *NSF-CAREER* award, DMR 0348884, and from a *Louisiana Board of Regents* grant, LEQSF (2002–05)-RD-A-09. We also acknowledge the support of *NIST* and the *NSF*, through agreement no. DMR 9986442 in providing the neutron research facilities used in this work. We thank Drs. *Igor Sics* and *Shaofeng Ran* for facilitating SAXS–WAXS measurements on beamlines X27C and X3(2A), respectively. The authors thank *J. M. Gloaguen* (LSPES, Lille, France) for performing cryo-ultramicrotome film preparations. We acknowledge the use of the *Socolofsky Microscopy Center* at Louisiana State University and the assistance of *Cindy Henk* in conducting microscopy.

- [1] [1a] S. S. Ray, M. Okamoto, *Prog. Polym. Sci.* **2003**, *28*, 1539; [1b] M. Alexandre, P. Dubois, *Mater. Sci. Eng. R* **2000**, *28*, 1.
- [2] G. Lagaly, *Appl. Clay Sci.* **1999**, *15*, 1.
- [3] H. Assender, V. Bliznyuk, K. Porfyrakis, *Science* **2002**, *297*, 973.
- [4] G. Schmidt, M. M. Malwitz, *Curr. Opin. Colloid Int.* **2003**, *8*, 103.
- [5] N. Ogata, S. Kawakage, T. Ogihara, *J. Appl. Polym. Sci.* **1997**, *66*, 573.
- [6] D. J. Chaiko, *Chem. Mater.* **2003**, *15*, 1105.
- [7] R. A. Vaia, S. Vasudevan, W. Krawiec, L. G. Scanlon, E. P. Giannelis, *Adv. Mater.* **1995**, *7*, 154.
- [8] B. van Duffel, R. A. Schoonheydt, C. P. M. Grim, F. C. De Schryver, *Langmuir* **1999**, *15*, 7520.
- [9] [9a] G. Decher, *Science* **1997**, *277*, 1232; [9b] G. Decher, J. Schlendorff, “*Multilayer Thin Films: Sequential Assembly of Nanocomposite Materials*”, VCH, Weinheim 2003.
- [10] [10a] E. R. Kleinfeld, G. S. Ferguson, *Science* **1994**, *265*, 370; [10b] P. Y. Vuillaume, K. Glinel, A. M. Jonas, A. Laschewsky, *Chem. Mater.* **2003**, *15*, 3625.
- [11] G. Schmidt, A. I. Nakatani, C. C. Han, *Rheol. Acta* **2002**, *41*, 45.
- [12] G. Schmidt, A. I. Nakatani, P. D. Butler, A. Karim, C. C. Han, *Macromolecules* **2000**, *33*, 7219.
- [13] G. Schmidt, A. I. Nakatani, P. D. Butler, C. C. Han, *Macromolecules* **2002**, *35*, 4725.
- [14] M. M. Malwitz, A. Dundigalla, V. Ferreiro, P. D. Butler, M. C. Henk, G. Schmidt, *Phys. Chem. Chem. Phys.* **2004**, *6*, 2977.
- [15] M. M. Malwitz, S. Lin-Gibson, E. K. Hobbie, P. D. Butler, G. Schmidt, *J. Polym. Sci., Part B: Polym. Phys.* **2003**, *41*, 3237.
- [16] V. Ferreiro, G. Coulon, *J. Polym. Sci., Part B: Polym. Phys.* **2004**, *42*, 687.
- [17] M. M. Malwitz, P. D. Butler, L. Porcar, D. P. Angelette, G. Schmidt, *J. Polym. Sci., Part B: Polym. Phys.* **2004**, *42*, 3102.
- [18] J. H. Wu, M. M. Lerner, *Chem. Mater.* **1993**, *5*, 835.
- [19] E. R. Kleinfeld, G. S. Ferguson, *Chem. Mater.* **1995**, *7*, 2327.
- [20] [20a] J. Lal, L. Auvray, *J. Appl. Crystallogr.* **2000**, *33*, 673; [20b] J. Lal, L. Auvray, *Mol. Cryst. Liq. Cryst.* **2001**, *356*, 503.
- [21] [21a] N. Ogata, S. Kawakage, T. Ogihara, *Polymer* **1997**, *38*, 5115; [21b] J. Bujdak, E. Hackett, E. P. Giannelis, *Chem. Mater.* **2000**, *12*, 2168.